Additive Manufacturing of a Steel–Ceramic Multi-Material by Selective Laser Melting

J. KOOPMANN, J. VOIGT, and T. NIENDORF

Most techniques employed for powder bed additive manufacturing (AM) only can handle a single material. However, additional functionality of the structures built, *e.g.,* local insulation, is desirable for more sophisticated applications. In the present work, a multi-material process allowing for realization of a ceramic coating on a steel substrate and a novel sandwich system are introduced. Both were manufactured by selective laser melting (SLM). As a first step, the microstructure of a bulk zirconia–alumina ceramic, directly manufactured by SLM, was examined and its tensile strength determined. Afterwards, the ceramic was manufactured directly on the as-built surface of a tool steel processed by SLM. For this compound, the adhesive strength was determined. Finally, an open porous structure, made of the same tool steel, was built on top of the ceramic layer. The results clearly prove that the SLM process can be used for direct manufacturing of a multi-material sandwich structure made from metal and ceramic, providing an important step towards complex structures functionalized for electric insulation.

https://doi.org/10.1007/s11663-019-01523-1

I. INTRODUCTION

ADDITIVE manufacturing (AM) is an emerging field and has recently gained significant attention in industry and academia. AM allows direct manufacturing of small-quantity batches and has the capability of producing highly complex structures and components. One of the most promising AM techniques is the selective laser melting (SLM) process, which has numerously proven to be suitable for production of metallic parts with nearly 100 pct density at low geometric restrictions. AM and SLM are comprehensively introduced in recent reviews, *e.g.* References 1 through 5.

In many industries, there is a high demand for combining different materials for the realization of tailored properties for specific applications. Multi-material design is the key not only for light-weight applications,[6] but also for functionalization of any given component, *i.e.*, the integration of actuators or sensors.[7] In the following, activities focusing on multi-material AM will be introduced. At this point, it is important to mention that the focus will be primarily on activities involving powder bed systems. So far, most work in AM of multi-materials has been conducted focusing on laser metal deposition (LMD) techniques.[8,9] It is obvious, that LMD is very efficient in terms of chemical gradation as the ratio of powder mixing can be easily set for a given processed volume. However, in terms of geometrical flexibility, LMD encounters limitations that can only be overcome by powder bed systems. In the latter case, the powder bed allows, *e.g.*, to support overhanging structures. In consequence, powder bed systems allow for direct manufacturing of molds with internal cooling channels of arbitrary shape. As such molds with integrated functionalities like sensors, actuators, or resistance heating elements are highly demanded by numerous industries, multi-material AM for powder bed techniques is a very promising field of research.

The use of powder bed AM techniques for multi-material components is often referred to as *multi-material printing,* being the focus of numerous research studies, *e.g.* Reference 5. One of the latest examples of *multi-material printing* is a work by Liu *et al.*[10] An interface between steel and copper was manufactured by selective laser melting, and good metallurgical bonding was obtained. Sing *et al.*[11] showed the formation of intermetallic phases in an aluminum–copper interface. A Fe/Al-12Si structure was manufactured by Gökhan-Demir and Previtali by mixing the powders in the SLM process.[12] These works clearly reveal the possibility of combining different metals in the SLM process. Another

J. KOOPMANN is with the Volkswagen AG, Group Research, Berliner Ring 2, 38436, Wolfsburg, Germany and also with the Institut für Werkstofftechnik (Materials Engineering), Mönchebergstr. 3, 34125 Kassel, Germany. Contact e-mail: Julian.Koopmann@volkswagen.de J. VOIGT is with the Volkswagen AG, Group Research. T. NIENDORF is with the Institut för Werkstofftechnik (Materials Engineering).

Manuscript submitted September 27, 2018.
Article published online February 6, 2019.

technical matter of importance is the fusion of ceramics and metals. Due to the extremely limited miscibility of ceramics and metals, manufacturing of interfaces with sufficient bond strength is very challenging. Other critical issues are delamination, caused by thermally induced stresses as being imposed by the different thermal expansion coefficients of metals and ceramics and poor wetting characteristics. Syed-Khaja and Franke[13] manufactured ceramic circuit carriers in the SLM process and proved the feasibility of processing metals on ceramics. In their study, they only melted the metal powder being used, *i.e.,* a bronze alloy, but not the ceramic, which was inserted as a solid build plate in the process. In light of free form fabrication and geometrical flexibility, the use of ceramic pre-forms impedes the realization of the full potential of AM techniques. Therefore, using ceramics in the form of powder and processing of these powders in a similar fashion as in case of the metals employed is highly desirable. Nagel[14] revealed the general possibility of laser welding of Al_2O_3. The laser welding process is somewhat similar to the SLM process (with respect to its local temperature–time history) and, thus, already indicates the possibility of processing at least alumina using AM techniques. This has been further substantiated by groups in Singapore and China reporting on the evolution of alumina upon single-track processing using SLM.[15,16] However, to the best of the authors' knowledge, the processing of bulk samples using alumina in the SLM process has not been reported to date.

As bulk ceramics can be used as dental implants, initial studies already addressed implications regarding the processability of ceramic powders by SLM. Wilkes[17] reported that a dry mixed powder of ZrO_2 and Al_2O_3 can be processed using the SLM process. The samples processed without preheating were reported to be characterized by a low strength, most probably due to numerous micro cracks in the specimens. As expected, ceramics processed at a preheating temperature of 1600 °C had a much higher strength due to the minimization of crack densities. Nevertheless, poor surface quality was observed.[17] Yttria partially stabilized (YPS) ZrO_2 has been manufactured at preheating temperatures in the range of 1500 °C to 2500 °C to investigate the influence of base-plate heating on crack formation.[18] The findings are in line with results on hard-to-process metallic alloys, where the absolute amount of processing induced defects could be significantly decreased by base-plate heating. By decreasing the temperature difference between the melt pool and the already solidified material, solidification and liquidation cracking can be reduced at least to a certain extent.[19] Furthermore, depending on the material deployed, the base-plate heating is only effective up to a given build height, again limiting design freedom of manufactured structures. The best results for a ceramic processed in a non-heated SLM chamber were obtained using a dry mixed powder with a weight ratio of 80 pct ZrO_2 and 20 pct Al_2O_3. The measured flexible strength was 9.5 ± 1.2 MPa, and complex geometries were built using this ratio of powder mixture.[17] In contrast to metals, ceramics are typically not molten due to their high melting temperatures. Instead the densification is realized by sintering, resulting in a characteristic microstructure.[20,21] For the SLM-processed ceramic, Wilkes[17] observed a dendritic microstructure. This indicates that the ceramic fully melted and rapidly solidified thereafter, which is also known from fusion casting[22] and Laser Engineered Net Shaping.[23]

For realization of functionally graded structures based on ceramics in combination with steel, a ceramic material characterized by a similar thermal expansion coefficient (as compared to steel) and robust processability using SLM without preheating is expected to be the most reasonable choice. A zirconia-based ceramic matches these requirements perfectly. Similar thermal expansion coefficients are provided in literature (steel $\alpha_{1000} = 12 \times 10^{-6}/K$[24] and ZrO_2 $\alpha_{1000} = 15.3 \times 10^{-6}/K$[25]) and the possibility of processing an adequate mixture of the zirconia-based material by SLM without preheating has been proven successfully as detailed above.[17]

Coatings made of oxide-ceramics are widely used in industrial applications. Thermal barrier coatings, *e.g.*, made of YPS–ZrO_2, are used in turbine engines for thermal insulation to improve engine efficiency.[24] Further applications of ceramic layers are wear-resistant coatings in engines and electrical insulation in the computer chip industry. All these ceramic coatings are mostly manufactured by plasma spray processes or physical vapor deposition (PVD).[24] In general, due to different atomic bonding and low wettability, the adhesion strength between ceramics and metals is low[21,26] and a mechanically interlocking system is beneficial in order to increase the adhesion strength.[24] Accordingly, the relatively rough surfaces produced in the SLM process, *e.g.*, detailed in References 27 through 29, could be an advantage for manufacturing ceramic coatings using a multi-material SLM process.

Syed-Khaja and Franke[13] showed the possibility of depositing metals on ceramic as already introduced above. A detrimental issue using bulk sheets of traditionally processed ceramic was delamination of the ceramic and metal surfaces due to different thermal expansions during manufacturing of the upper steel layer. In their study, the authors only tried to reduce the heat input in the ceramic by manufacturing an open porous upper steel layer; however, they did not modify the surface layer in between the ceramic and the steel.

The current study was carried out to close this research gap. First, a multi-material SLM process is used to manufacture a ceramic layer on an AM steel substrate. Besides, the development of process parameters for the ceramic itself and appropriate strategies for strengthening the ceramic–steel interlayer are established. Finally, a sandwich structure following the architecture *steel–ceramic–steel* was successfully processed. Thereby, for the first time it is proven that a functionally graded compound made from ceramics and steel solely using the SLM process at ambient temperature can be obtained. In future applications, this will allow for the realization of electric insulation in tools as well as integration of sensors or actuators not impeding the inherent advantages of the AM processes. Steps to

be accomplished towards this goal, particularly the perpetuation of the geometrical design freedom, will be briefly summarized in the outlook section.

II. EXPERIMENTAL DETAILS

A. *Experimental Setup*

All specimens were manufactured using a Realizer SLM 125 machine. Design data for the processed structures were compiled using the software Materialise Magics and Realizer RDesigner. The maximum power output of the fiber laser (wavelength = 1070 nm) is 422 W with a focus diameter of 150 μm, measured by Cinogy Focus Beam Profiler. The machine is equipped with a high-temperature substrate plate for heating up to 500 °C. For the current study, ceramic and metal powders were processed separately, *i.e.*, only one material was used in the machine at a given time. Thus, no issues prevailed in separating the powders after the build. More information on future machine design and implementation of a multi-material SLM process is given in the outlook section of this work. The Realizer SLM 125 allows for the variation of spot distance and pulse time to vary the scan velocity. By neglecting the motion time, the scan speed (v_s) is determined by

$$v_s = \frac{\text{spot distance [m]}}{\text{pulse time [s]}}.$$

Cubic samples with dimensions of 10 mm × 10 mm × X mm were manufactured. The height X of each layer is dependent on the stacking architecture of the single specimen. Detailed information on overall sample dimensions and processing parameters is presented in the respective part of the *Results and Discussion* section only for the sake of clarity.

III. MATERIALS

Two initial materials were used in the experiments. A 1.2367 (X38CrMoV5-3) tool steel powder, supplied by H.C. Starck GmbH, Germany, was used as the metallic base material. The steel has already been successfully employed in SLM[30] and is a balanced choice for tooling applications. As one key application envisaged is the production of functionalized tools processed by AM, integration of electric insulation layers directly in the manufacturing process using this single base metal has been considered here as a first step towards robust multi-material SLM. The powder has been gas atomized and is characterized by a spherical shape with a powder particle size of 10 to 63 μm and a median size of 28.6 μm. The ceramic powder used was obtained by dry mixing of two initial components with a weight ratio of 80 pct ZrO_2 and 20 pct Al_2O_3. Both ceramic powders were supplied by ceram GmbH Ingenieurkeramik, Germany. The equilibrium phase diagram of the ZrO_2-Al_2O_3 system is given in Figure 1 for general evaluation of the composition of the chosen mixture. Phase diagrams accounting for the rapid solidification and cooling are not available in open literature, yet, while the calculation of such a diagram is clearly beyond the scope of the current study.

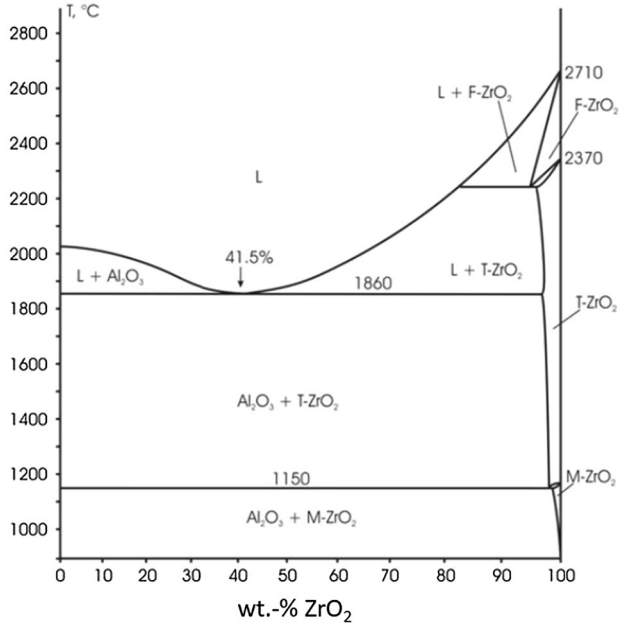

Fig. 1—Phase diagram of the system Al_2O_3-ZrO_2. Reprinted with permission from Ref. [31].

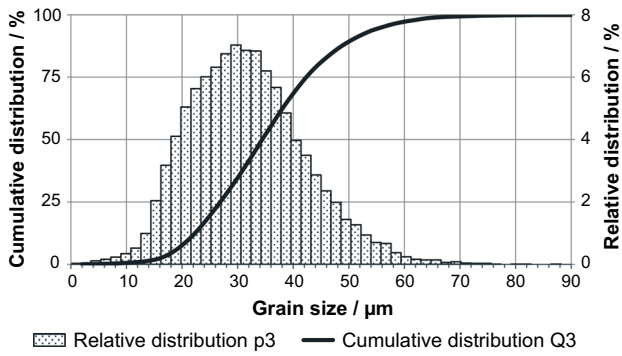

Fig. 2—Cumulative and relative distribution of the particle size of the dry mixed ceramic powder.

The size distribution of the mixed ceramic powder was measured employing a Retsch Camsizer XT. The median of the equivalent diameter, defined as the equivalent diameter of a sphere with the same area as the measured particle, was 34.5 μm (Figure 2). The sphericity of the particles is determined by the b/l-ratio of 0.77, where b is the smallest dimension of the particle and l is the largest.

A. *Microstructure and Property Analysis*

For characterization of the microstructure, the samples were cut from the building platform and embedded. Mechanical grinding employed papers of 120, 40, 15, and 10 μm grit size. Afterwards, the samples were polished with diamond solutions of 6 and 3 μm. A Keyence VHX-5000 was used for optical imaging and determination of the relative density of samples built.

A FEI Scios Dual Beam scanning electron microscope (SEM) was used for microstructure investigations and EDS analysis. For the SEM micrographs shown in this work, an acceleration voltage of 20 kV and secondary electron contrast were used. The ceramic samples were sputtered with gold in order to form a thin layer guaranteeing electric conductivity.

The samples manufactured for tensile testing of the bulk ceramic were processed according to the geometries given in Figure 3. All tests were conducted in as-built condition without any post treatment. The tensile tests were done with a DeFelsko PosiTest AT pull-off tester with a loading rate of 2 MPa/s. The dolly head was adhered to the top surface of the specimen using HTK Ultra Bond 100, the bottom surface was maintained on the build plate. For determination of the adhesive strength between ceramic and steel layers, the samples were manufactured in two parts. The lower half of the sample (Figure 3) was manufactured with steel, then the material was changed, and the ceramic was added starting from the middle of the overall height of the sample (the position highlighted by the horizontal arrow indicating the sample diameter).

For determining the volumetric electrical resistance of the SLM-manufactured ceramic, an N&H Technology Hiresta UX equipped with a UR-SS measuring head was used. The sample geometry used in these tests was a cube featuring dimensions of 10 mm $\times$ 10 mm $\times$ 10 mm.

IV. RESULTS AND DISCUSSION

A. *SLM Processing of the Ceramic Powder*

Ceramic specimens featuring dimensions of 10 mm $\times$ 10 mm $\times$ 10 mm were built using a variety of manufacturing parameters. The scan velocity was varied between 50 and 310 mm/s and the hatch distance was set between 50 and 330 μm in order to determine the parameters leading to the highest relative density. Evaluation of structural integrity and surface appearance of the as-built structures allowed for the selection of the most adequate SLM processing parameter set. The specimens used for optical imaging (Figure 4) were processed as already detailed in the experimental part. The apparent relative density was determined by light microscopy. The determined parameter used for processing of ceramic in the remainder of the work comprises a relatively low laser power of 90 W, a scanning velocity of 200 mm/s, a hatch distance of 160 μm, and a layer thickness of 50 μm. For the sake of brevity, the full matrix detailing all process parameter combinations employed is not shown. However, the conclusions of the parameter study can be briefly summarized as follows: At high power, the ceramic evaporates, for low power unmolten areas are observed as already described by Wilkes.[17] The maximum relative density obtained for the ceramic samples based on the set of parameters provided above was approximately 94 pct.

The experimentally determined volumetric electrical resistance of the SLM-processed ceramic including all structural features detailed in the following was 2.84×10^{10} Ωcm, a value being sufficient for electric insulation according to Ivers-Tiffée *et al.*[32]

The tensile strength (sample geometries are shown in Figure 3 in the experimental section), which has been determined using five specimens, was 20.4 $\pm$ 4.6 MPa. This is in good agreement with the measured flexural

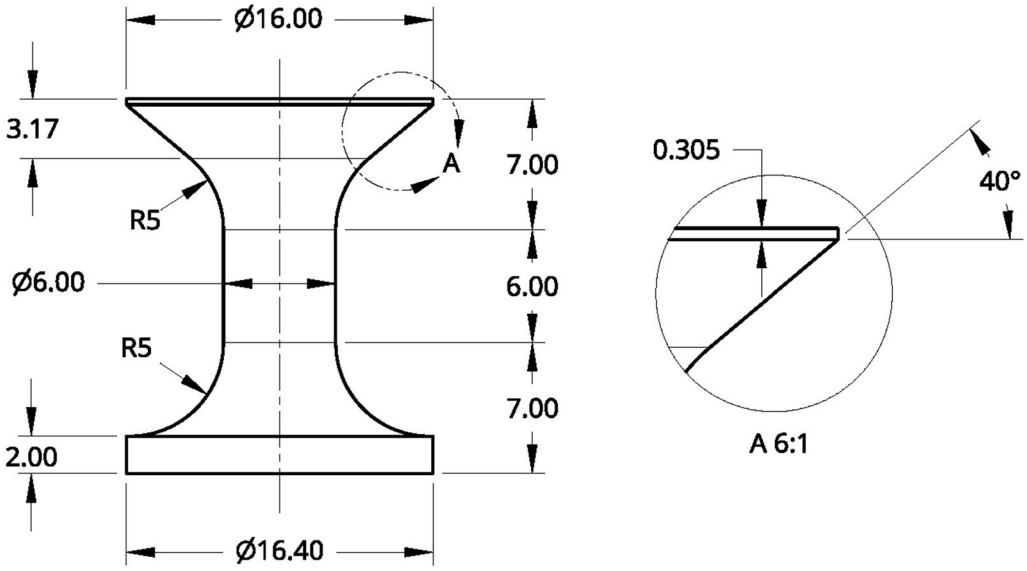

Fig. 3—Schematic detailing the dimensions of the samples used for mechanical property tensile testing.

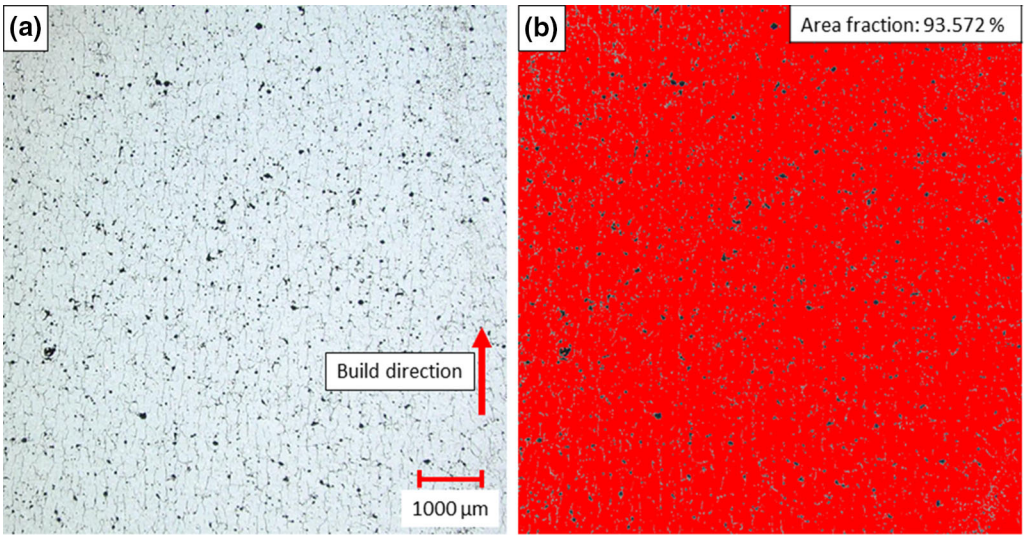

Fig. 4—(*a*) Overview micrograph showing a ground and polished ceramic sample. (*b*) Density measurement of the ceramic sample based on microscopic data (red: solid material, black: pores) (Color figure online).

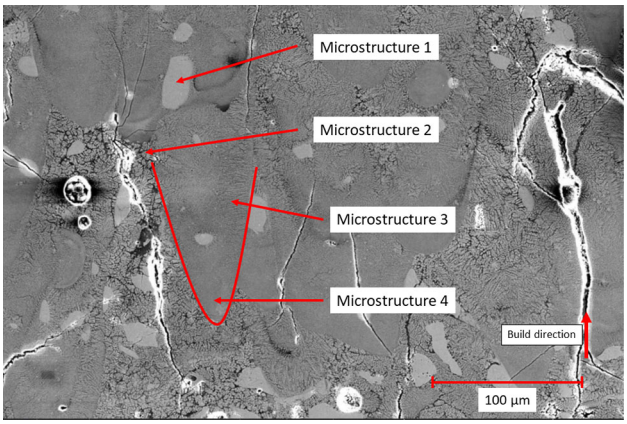

Fig. 5—SEM micrograph revealing the heterogeneous microstructure of the SLM-manufactured ceramic.

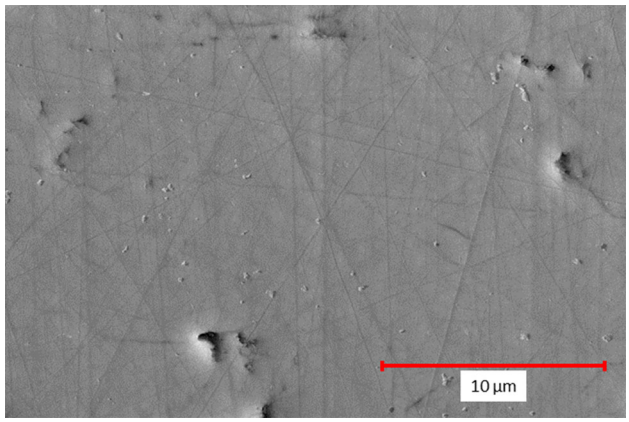

Fig. 6—SEM-image of an unmolten as-delivered zirconia powder particle.

strength (9.5 ± 1.2 MPa) in the 4-point bending tests (sample geometries: 46.6 mm × 6 mm × 5.5 mm) reported by Wilkes.[17] The scatter of data is in an acceptable range and, thus, indicates good reproducibility of bulk properties for the ceramic processed *via* SLM.

Microstructural analysis by SEM revealed the formation of basically four microstructures, each one different in appearance, within a single melting line of the ceramic (Figure 5). For one melt pool, the melt pool boundary is highlighted by a red line (Figure 5). Details from each microstructure, highlighted by the red arrows in Figure 5, are shown in high resolution in Figure 7. From the overview image shown in Figure 5, important aspects can already be deduced: Unmolten ceramic particles featuring the microstructure seen in the initial powder, separately depicted in Figure 6, are partly present in the sample (Microstructure 1; Details in Figure 7(a)). In the upper region of the melt pool (Microstructure 2; Details in Figure 7(b)), a relatively coarse microstructure can be seen as compared to the microstructure in the lower region (Microstructure 4; Details in Figure 7(d)). The difference is assumed to be caused by faster solidification in the lower region resulting in finer dendritic structures, which have been shown numerously in metallic alloys.[33] Microstructure 3 (Details in Figure 7(c)) is a transition zone and the cooling rate and the resulting size of microstructural features is in between Microstructure 2 and Microstructure 4, thus, again resembling a dendritic structure.

EDS was employed to reveal the distribution of the elements within the different microstructures. The interdendritic regions are enriched with alumina (Figure 8). This is thought to be induced by the non-equilibrium solidification due to the high cooling rates and an enrichment of alumina in the remaining liquid phase during solidification. Generally, a partially eutectic solidification mode is revealed for the SLM-processed blend of the two elementary ceramic powders. This could be already expected from the equilibrium phase diagram (Figure 1). However, the results cannot be

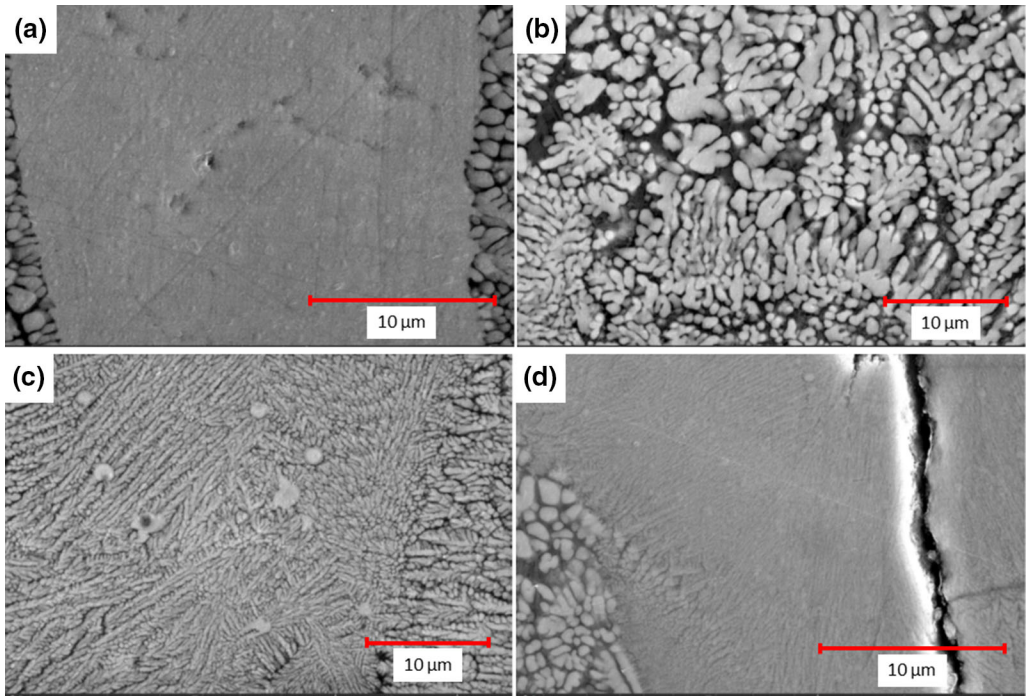

Fig. 7—The four microstructures ((*a*) Microstructure 1, (*b*) Microstructure 2, (*c*) Microstructure 3, (*d*) Microstructure 4) in the ceramic specimens recorded at high resolution. The distribution of these microstructures within the former melt pool is indicated in Fig. 5.

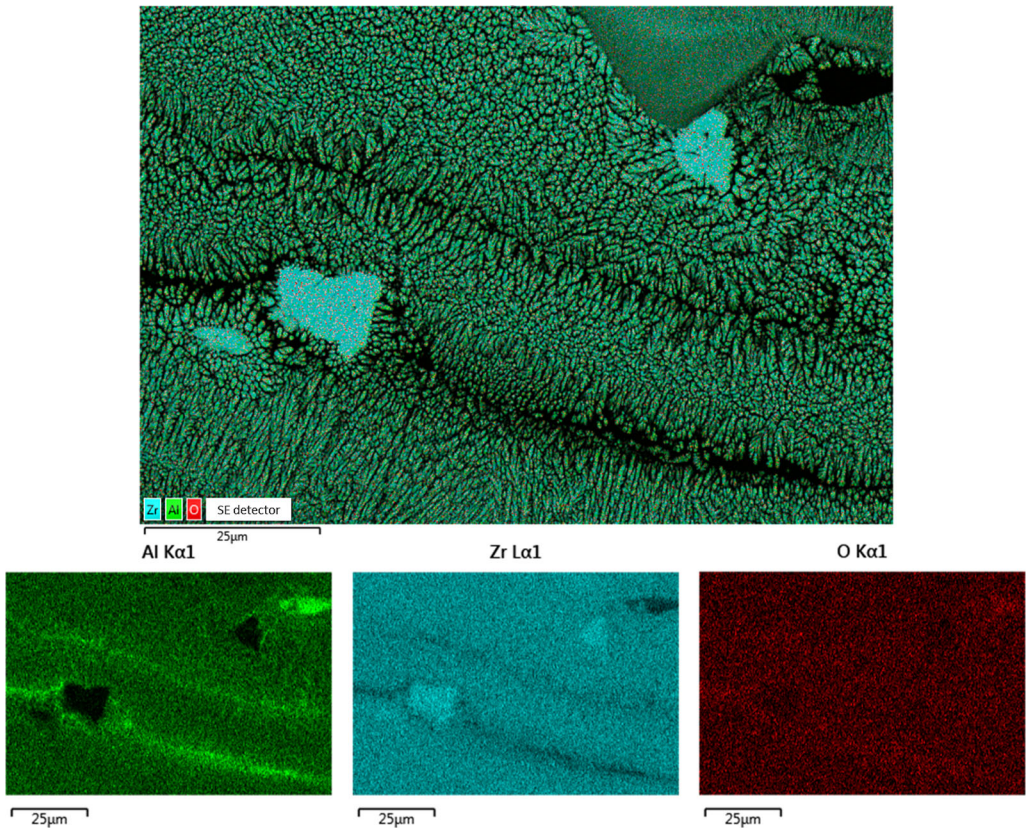

Fig. 8—EDS element mappings revealing the distribution of Al, Zr, and O in the ceramic microstructure.

directly transferred due to the significantly higher (non-equilibrium) solidification upon SLM. As already detailed before, calculation of a phase diagram resembling the prevailing cooling conditions during SLM is beyond the scope of the current work; however, this will have to be conducted in the future for a more detailed evaluation of microstructure evolution in the ceramic.

B. *Processing of a Ceramic Layer on an AM Steel Substrate*

Ceramic layers were manufactured on the top of 10 mm × 10 mm × 4 mm SLM steel substrates. In a first series of experiments, the whole ceramic layer was manufactured employing the parameters for highest density detailed above. This leads to a characteristic inter-material layer with hollow areas and insufficient bonding between the steel and the ceramic (Figure 9), resulting in severe lack of fusion.

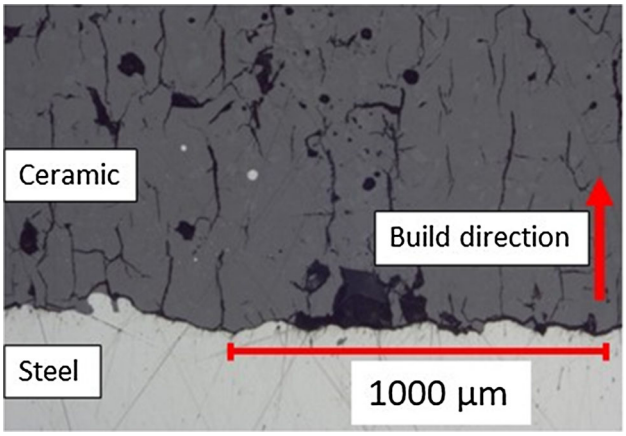

Fig. 9—Steel–ceramic interface where the ceramic layer (dark gray, upper part) was processed with a single set of processing parameters. The black line separating ceramic and steel is a large lack of fusion zone. See text for details.

In order to improve bonding in between steel and ceramic, process parameters employed in SLM were adjusted. Yu *et al.*[34] demonstrated that laser re-melting of a plasma-sprayed ceramic layer can significantly improve the steel–ceramic interface in terms of adherence. This strategy was transferred to the current SLM process. A first ceramic layer of 0.15 mm thickness was dispensed on top of the steel substrate. The process parameters employed for melting this initial ceramic layer comprised a power of 90 W, a scanning velocity of 270 mm/s, a hatch distance of 150 μm, and a powder layer thickness of 50 μm, *i.e.,* the parameters used for maximum density as detailed above. This 0.15-mm-thick ceramic layer as well as the uppermost part of the steel were then re-melted by a laser beam of much higher power, *i.e.*, 422 W according to the maximum power available in the SLM system used. Re-melting was conducted using a scanning velocity of 750 mm/s and a hatch distance of 70 μm. Further ceramic layers added thereafter were built using the parameters for highest density mentioned above.

As intended, re-melting of the initial ceramic layer by the high-power laser beam not only affected the ceramic layer but also re-melted the upper parts of the steel layer. Due to the well-known turbulences in the melt pool, *e.g.,* induced by Marangoni convection, a serrated surface between the steel and the ceramic coating resulted. This led to a significant improved bonding between the steel and the ceramic layer. The interface revealing well-defined interlocking is shown in Figure 10. Obviously, a good bonding between the two materials without traces of lack of fusion is observed. This is thought to be imposed by two interrelated aspects: The serrated surface leads to a form-locking interface connection while it simultaneously diminishes the thermally induced stresses between steel and ceramic layers due to a breakdown of the effective boundary surface length (with respect to a given straight orientation). EDS clearly reveals that no diffusion of iron or ceramic into each other occurred and, thus, substance-to-substance bonding due to diffusion can be neglected (Figure 11).

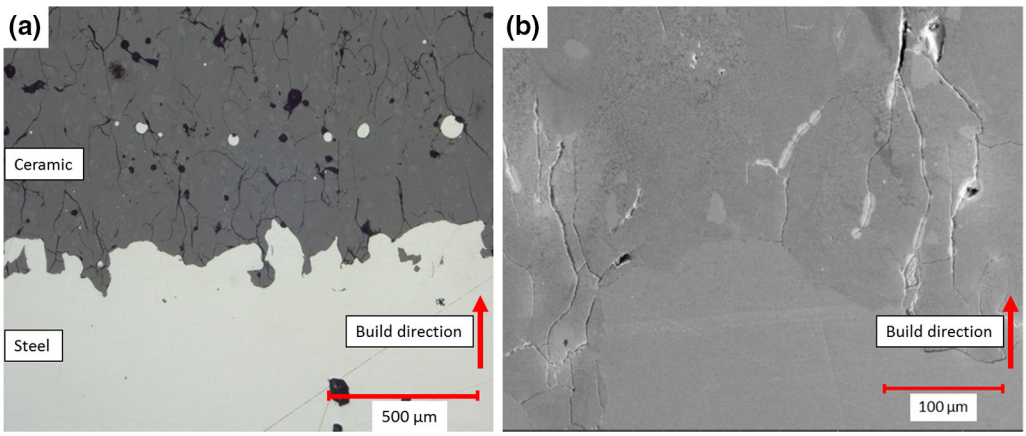

Fig. 10—(*a*) Steel–ceramic interface processed using a re-melting strategy and (*b*) SEM micrograph revealing good adhesion between steel and ceramic. In both micrographs, the ceramic layer is on the top. See text for details.

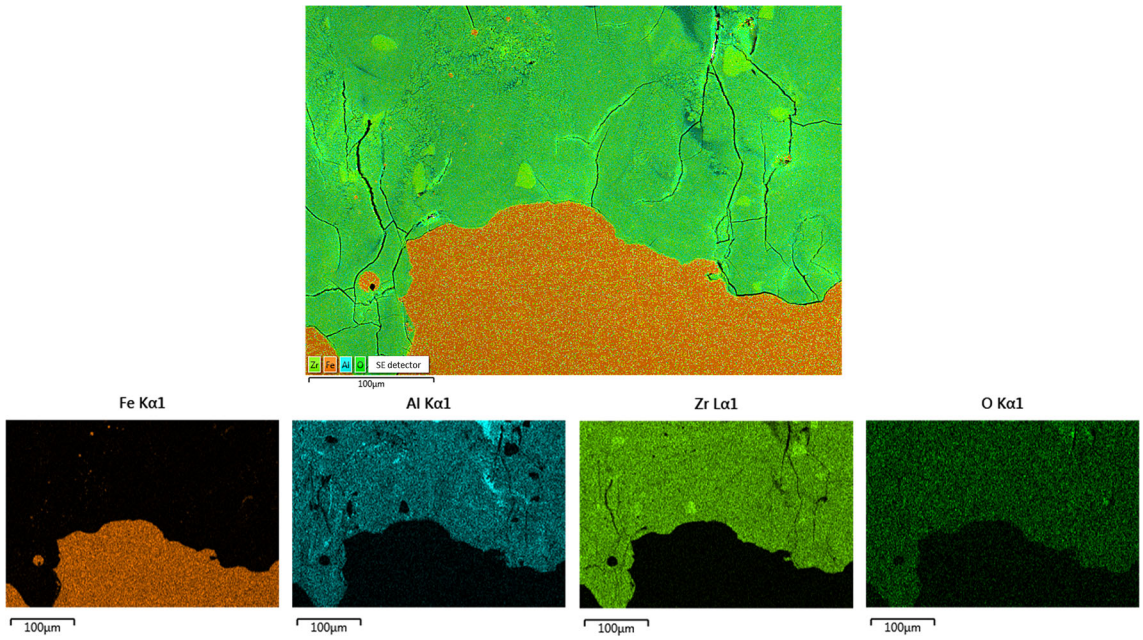

Fig. 11—EDS element mappings revealing the distribution of Fe, Al, Zr, and O in vicinity of the steel–ceramic interface.

The adhesion strength was determined based on five tensile tests. The sample dimensions used are provided in the experimental section. The tensile strength experimentally determined for the ceramic–steel specimens, manufactured by the advanced processing scheme including the re-melting cycle, was 22 ± 4.4 MPa. The failure occurred directly at the interface. This value for the adhesion strength, however, is in the same range as the determined tensile strength of the ceramic clearly revealing good bonding.

For analyzing the influence of the high-power laser treatment, the tensile strength of samples processed with a second set of re-melting parameters was examined: a laser power of 422 W, scanning velocity of 750 mm/s, and a ten times larger hatch distance of 700 μm (as compared to the condition presented before) were considered. The determined tensile strength was 6.7 ± 0.7 MPa, clearly, indicating that the optimized high-power laser treatment of the steel–ceramic interface detailed before increased the adhesion strength significantly. Employing the hatch distance of 700 μm, increased adhesion strength is only found in some areas of the sample. The fracture surface shown in Figure 12 reveals traces of good adhesion of ceramic (dark gray lines, one line being highlighted by a red arrow) on the steel surface every 700 μm, *i.e.*, following the used hatch distance.

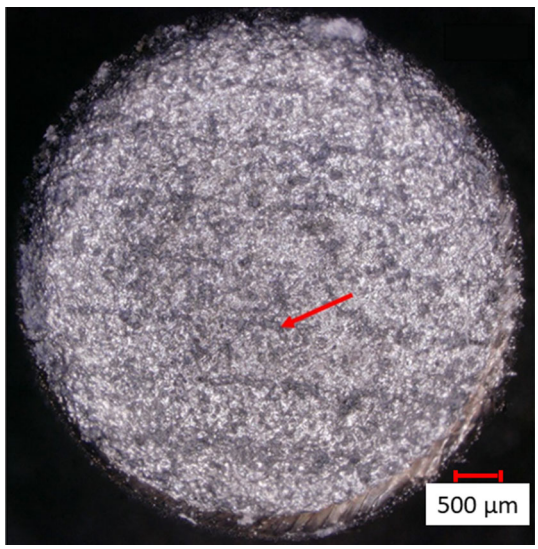

Fig. 12—Fracture surface of a steel–ceramic bi-layer sample. The sample was tensile tested and the surface shown is from the steel part of the sample. Remaining ceramic on the fracture surface shows up in the form of gray lines, one being marked by the red arrow (Color figure online).

C. *Processing of the Functionally Graded Steel–Ceramic–Steel System*

Finally, a sandwich structure, *i.e.*, a layered steel–ceramic–steel structure, was manufactured by SLM. The processing parameters used for SLM manufacturing of bulk steel directly on the build platform, *i.e.*, the standard parameters for the steel, led to delamination of the lower steel–ceramic interface, *i.e.*, the layer presented and discussed in the previous paragraph, when employed for processing of the uppermost steel layer. Lower laser energy resulted in insufficient bonding at the new (upper) interlayer between the ceramic and the steel.

The reason for the delamination is thought to be induced primarily by the differences in thermal expansion resulting in high interlayer surface stresses between the steel and the ceramic and poor adhesion strength as discussed before. Besides delamination, balling-effects appeared during manufacturing of the steel. This is due to several reasons. The melting temperature of the

ceramic is much higher than the melting temperature of the steel so that the lower ceramic layer assumedly did not re-melt. This leads to a relative smooth surface characterized by low bond strength as discussed before. Furthermore, the ceramic layer is characterized by its heat insulating properties. Thus, thermal flux is changed significantly, leading to a high probability of overheating the steel layer.

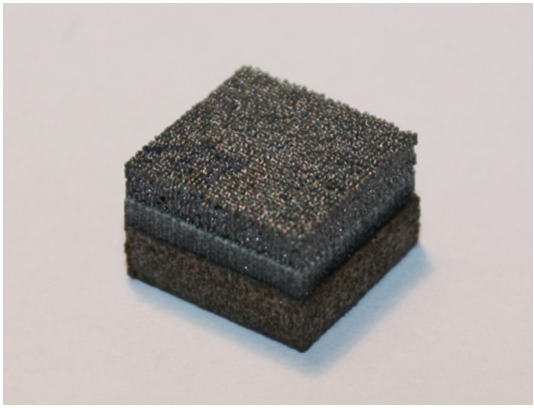

Fig. 13—Tri-layer sandwich structure featuring a 10-mm base and a height of approximately 7 mm. The initial steel substrate is shown at the bottom, a ceramic layer in the middle, and a steel open porous grid structure on the top.

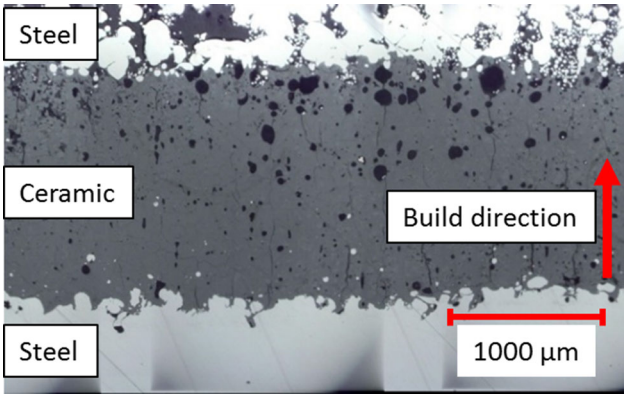

Fig. 14—Cross section of the sandwich structure shown in Fig. 13 with upper and lower steel layers embedding the ceramic layer (dark gray) in the middle.

To prevent these issues, the steel added on top of the ceramic was realized as an open porous structure to reduce the absolute volumetric energy input into the ceramic. This has been realized purely based on adjustment of processing parameters, *i.e.*, by an increase of the hatch distance of the steel to 250 μm (not the adaption of the geometry of the structure itself). Structural integrity of the lower steel–ceramic interface revealed that the ceramic did not heat up as much as in the case of manufacturing a bulk homogenous steel layer. This eventually led to a reduction of thermal stresses between the steel and the ceramic. Furthermore, a larger hatch distance of 240 μm during SLM processing of the ceramic was used. This resulted in the evolution of a less dense structure, in which stresses could be lowered due to the potential opening of cracks. As it is known from high-temperature material coatings used, for example, in turbine applications,[24] these small cracks allow for thermal expansion and contraction without leading to critical local stresses finally destroying the whole ceramic layer.

The tri-layer steel–ceramic–steel structure with the initial steel substrate on the bottom, the ceramic layer in the middle, and the open porous structure on the top is shown in Figure 13. In Figure 14, the cross section of the ground and polished sandwich structure is shown. Cracks near the lower interface are present, however, sufficient bonding between the ceramic and the steel substrate promotes structural integrity of the whole structure. Figure 15 reveals that not only good bonding at the lower steel–ceramic interface but also the upper ceramic–steel (open porous structure) interface is established. In both cases, surfaces are serrated and, thus, provide a good bonding strength.

V. CONCLUSION AND OUTLOOK

This present work demonstrates the feasibility of manufacturing functionally graded structures combining metal and ceramic systems in a multi-material SLM process. Based on a thorough process and parameter development, layered structures of sufficient structural integrity for the envisaged functionalized tooling applications were obtained. Regarding processing of tri-layer structures for direct manufacturing of insulation layers within a single process, the following conclusions can be drawn:

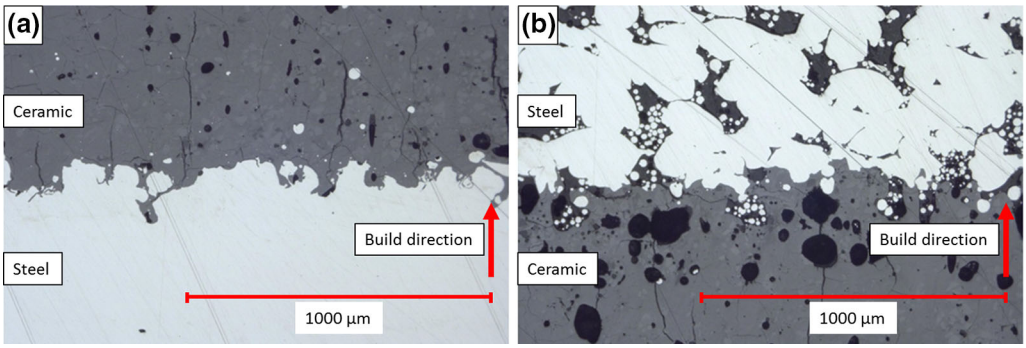

Fig. 15—(*a*) Lower steel–ceramic interface and (b) upper ceramic–steel interface at higher magnification.

- The microstructure of the ceramic compound mixed from elementary alumina and zirconia powders consisted of four different microstructures. These different microstructures were caused by different cooling rates during manufacturing in the SLM process and unmolten zirconia powder particles. The tensile strength of the ceramic was 20.4 ± 4.6 MPa and the volumetric electrical resistance was 2.84×10^{10} Ωcm. Both values are sufficient for the envisaged application.
- Good bonding at the metal–ceramic interface was achieved by establishing a serrated interlayer boundary by re-melting the interface area. Furthermore, realization of an open porous metal structure on top of the ceramic promoted good bonding. The measured adhesion strength was 22 ± 4.4 MPa, being very similar to the tensile strength of the ceramic.
- For further optimization of the multi-material SLM process, the powder system has to be modified. Integration of a new powder deposition system for locally defined deposition of the intended material has to be accomplished to produce parts consisting of multiple materials, while retaining the design freedom of the SLM process. This kind of system needs to be able to change the powder in a non-interrupted process and, thus, will combine the advantages of SLM and LMD.
- Finally, for integrating electrical circuits and sensors more than two different materials have to be processed simultaneously in the SLM process. Depending on the layer architecture and overall geometry of the component, processing parameters need to be adapted locally. Thus, comprehensive knowledge of the relationships between processing strategy, layer architecture, and component geometry as well as electrical characteristics and mechanical properties need to be established.

REFERENCES

1. W. Meiners: Direktes selektives Laser-Sintern einkomponentiger metallischer Werkstoffe, Dissertation, Aachen, 1999.
2. I. Gibson, D. Rosen, and B. Stucker: *Additive Manufacturing Technologies*, 2nd ed., Springer, New York, 2009.
3. A. Gebhardt and J.-S. Hötter: *Additive Manufacturing: 3D Printing for Prototyping and Manufacturing*, Carl Hanser Verlag, München, 2016.
4. D. Herzog, V. Seyda, E. Wycisk, and C. Emmelmann: *Acta Mater.*, 2016, vol. 117, pp. 371–92.
5. T. DebRoy, H.L. Wei, J.S. Zuback, T. Mukherjee, J.W. Elmer, J.O. Milewski, A.M. Beese, A. Wilson-Heid, A. De, and W. Zhang: *Prog. Mater. Sci.*, 2018, vol. 92, pp. 112–224.
6. E. Malone and H. Lipson: in *Proceedings of the ASME 2008 9th Biennial Conference on Engineering Systems Design and Analysis*, 2008, pp. 345–53.
7. D. Lehmhus, C. Aumund-Kopp, F. Petzoldt, D. Godlinski, A. Haberkorn, V. Zöllmer, and M. Busse: *Procedia Technol.*, 2016, vol. 26, pp. 284–301.
8. F. Brueckner, A. Seidel, E. Lopéz, C. Leyens, and E. Beyer: *Solid Free. Fabr. Symp.*, 2017, pp. 2530–38.
9. M. Vaezi, S. Chianrabutra, B. Mellor, and S. Yang: *Virtual Phys. Prototyp.*, 2013, vol. 8, pp. 19–50.
10. Z.H. Liu, D.Q. Zhang, S.L. Sing, C.K. Chua, and L.E. Loh: *Mater. Charact.*, 2014, vol. 94, pp. 116–25.
11. S.L. Sing, L.P. Lam, D.Q. Zhang, Z.H. Liu, and C.K. Chua: *Mater. Charact.*, 2015, vol. 107, pp. 220–27.
12. AG Demir and B Previtali: *Manuf. Lett.*, 2017, vol. 11, pp. 8–11.
13. A. Syed-Khaja and J. Franke: in *Proceedings of Electronic Components and Technology Conference*, 2016, pp. 837–42.
14. A.-M. Nagel and H. Exner: in *Proceedings of SPIE—International Society for Optical Engineering*, 1999.
15. K. Zhang, T. Liu, W. Liao, C. Zhang, D. Daozhong, and Y. Zheng: *Optik (Stuttg)*, 2018, vol. 156, pp. 487–97.
16. Z. Fan, L. Mingyuan, and H. Huang: *Ceram. Int.*, 2018, vol. 44, pp. 9484–93.
17. J.I. Wilkes: Selektives Laserschmelze zur generativen Herstellung von Bauteilen aus hochfester Oxidkeramik, Dissertation, Aachen, 2009.
18. Q. Liu, Y. Danlos, B. Song, B. Zhang, S. Yin, and H. Liao: *J. Mater. Process. Technol.*, 2015, vol. 222, pp. 61–74.
19. J. Krell, A. Röttger, K. Geenen, and W. Theisen: *J. Mater. Process. Technol.*, 2018, vol. 255, pp. 679–88.
20. H.L. Calambás Pulgarín and M.P. Albano: *Procedia Mater. Sci.*, 2015, vol. 8, pp. 180–89.
21. A. Baumann: Pulverspritzgießen von Metall-Keramik-Verbunden, Dissertation, Freiberg, 2010.
22. A.M. Alper: in *Ceramic Microstructures: Their Analysis, Significance, and Production*, R.M. Fulrath and J.A. Pask, eds., Wiley, New York, 1969, pp. 763–99.
23. F. Niu, W. Dongjiang, G. Ma, J. Wang, J. Zhuang, and Z. Jin: *Procedia CIRP*, 2016, vol. 42, pp. 91–95.
24. R. Bürgel: *Handbuch Hochtemperatur-Werkstofftechnik*, 3rd ed., Friedrich Vieweg & Sohn Verlag, Wiesbaden, 2006.
25. N. Mesrati, H. Ajhrourh, N. Du, and D. Treheux: *J. Therm. Spray Technol.*, 2000, vol. 9, pp. 95–99.
26. K. Suganuma, Y. Miyamoto, and M. Koizumi: *Weld. Int.*, 1987, vol. 1, pp. 875–78.
27. M. Leary: *Surface Roughness Optimisation for Selective Laser Melting (SLM): Accommodating Relevant and Irrelevant Surfaces*, Elsevier, 2016.
28. J.C. Fox, S.P. Moylan, and B.M. Lane: *Procedia CIRP*, 2016, vol. 45, pp. 131–34.
29. G. Strano, L. Hao, R.M. Everson, and K.E. Evans: *J. Mater. Process. Technol.*, 2013, vol. 213, pp. 589–97.
30. W. Kniffka, M. Eichmann, G. Witt, and R. Stache: in *Rapid. Tech Int. Trade Show Conference for Additive Manufacturing*, W. Kniffka, G. Witt, and M. Eichmann, eds., Carl Hanser Verlag GmbH & Co. KG, 2016, pp. 380–89.
31. S.M. Lakiza and L.M. Lopato: *J. Am. Ceram. Soc.*, 1997, vol. 80, pp. 893–902.
32. E. Ivers-Tiffée and W. von Münch: *Werkstoffe Der Elektrotechnik*, 9th ed., Vieweg + Teubner Verlag, Wiesbaden, 2004.
33. C.H. Cáceres, C.J. Davidson, J.R. Griffiths, and C.L. Newton: *Mater. Sci. Eng. A*, 2002, vol. 325, pp. 344–55.
34. Yu. Jianbing, Y. Wang, F. Zhou, L. Wang, and Z. Pan: *Appl. Surf. Sci.*, 2018, vol. 431, pp. 112–21.